Theoretical Investigation of the Magnetic Interactions of Ni_9 Complexes

Mitsuo Shoji,* Yasutaka Kitagawa, Takashi Kawakami, Shusuke Yamanaka, Mitsutaka Okumura, and Kizashi Yamaguchi

Department of Chemistry, Graduate School of Science, Osaka University, Machikaneyama 1-1, Toyonaka, Osaka 560-0043, Japan

Received: December 6, 2007; In Final Form: January 16, 2008

On the basis of density-functional theory (DFT) calculations, a theoretical analysis of the exchange interactions in $Ni_9L_2(O_2CMe)_8\{(2\text{-py})_2CO_2\}_4$, was performed, where L is a bridging ligand, OH^- (**1**) or N_3^- (**2**). Each magnetic interaction between the Ni spin centers is analyzed for **1** and **2** in terms of exchange integrals (*J* values), orbital overlap integrals (*T* values) and natural orbitals. It was found that a J_3 interaction, which is a magnetic interaction via the bridging ligand orbitals, mainly controls the whole magnetic properties, and the dominant interaction is a σ-type orbital interaction between Ni d_{z^2} orbitals. Further investigations on the magnetostructural correlations are performed on the J_3 interactions using simplest Ni−L−Ni models. These models reproduced the magnetic interactions qualitatively well not only for the Ni_9 complexes but also for other inorganic complexes. Strong correlations have been found between the magnetic orbital overlaps (*T* values) and the Ni−L−Ni angle. These results revealed that the difference of the magnetic properties between OH^- and N_3^- is caused by the orbital overlap integral (*T* values) of the σ-type J_3 interaction pathway. The magnetic interactions are also discussed from a Hubbard model by evaluating the transfer integral (*t*) and on-site Coulomb integrals (*U*), in relation to the Heisenberg picture.

1. Introduction

Multinuclear metal complexes have attracted much attention in recent years for their material properties and reactivity. One of the most exciting developments in material science is a discovery of single molecule magnets (SMMs), which show quantum phenomenological magnetic properties.[1−3] At low temperature, SMMs show stepwise magnetizations caused by a quantum magnetization tunneling (QMT). SMMs provide an ideal opportunity to investigate quantum mechanical properties. SMMs are also expected as nanosized information storages for the slow relaxation property of magnetization at low temperature. The ground spin state becomes bistable in case of negative *D* value, where *D* is the anisotropy constant. The bistable spin states, spin-up and spin-down states, are separated by anisotropy energy barrier approximately given by $|D|S^2$, where *S* indicates the ground spin size. Thus it is necessary to design a SMM complex with a large *S* and a negatively large *D* for applications.[4]

In recent years, variety of SMMs have been discovered, and the number of SMMs continues to increase. Therefore, it is important to analyze the electronic structures and magnetic properties of the multinuclear metal complexes both experimentally and theoretically.

Multinuclear metal complexes composed of nine Ni atoms, $[Ni_9L_2(O_2CMe)_8\{(2\text{-py})_2CO_2\}_4]$, where the ligand L = OH (**1**) or N_3 (**2**), were synthesized as candidates for SMMs.[7,8] Interestingly, the magnetic properties of the Ni complex (Ni_9) change depending on the bridging ligand L. The ground spin states were reported to be $S = 1$ and 9 for **1** and **2**, respectively.[8] The molecular structures are shown in Figure 1. These magnetic properties are very important because whole molecular magnetism could be controlled by the ligands. Temperature-dependent magnetic susceptibility (χT) measurements revealed the magnetic interactions (*J* values) for **1**.[8] On the other hand, *J* values for **2** were not determined experimentally.

TABLE 1: Four Broken Symmetry Spin States of the Ni_9 Complexes Calculated in This Study[a]

spin state	S_z[a]	S_1	S_2	S_3	S_4	S_5	S_6	S_7	S_8	S_9
1	9	+1	+1	+1	+1	+1	+1	+1	+1	+1
2	7	−1	+1	+1	+1	+1	+1	+1	+1	+1
3	1	+1	+1	−1	+1	−1	+1	−1	+1	−1
4	1	+1	+1	+1	−1	−1	+1	+1	−1	−1

[a] Local spin distributions at the Ni spin centers are listed. [b] *z* component of the total spin angular momentum.

In our previous report, all the exchange interactions of **1** and **2** were evaluated by density functional theory (DFT) calculations, and theoretical analyses for *J* values were performed in direct comparison to the experimental χT curves.[9] The calculated *J* values for **1** were consistent with experimental results. However, the calculated J_3 value for **2** was out of an average *J* value for other similar dinuclear Ni complexes, where J_3 is a magnetic interaction through the bridging ligand, azido. At the calculated *J* values for **2**, the ground spin state was concluded to be $S = 1$ for a calculated weak antiferromagnetic J_3 value. Therefore, detailed theoretical investigation of the magnetic interactions is necessary.

In this study, theoretical analysis of magnetism and electronic structure of the Ni_9 complexes (**1, 2**) is performed by first principle method at hybrid density functional theory (HDFT) level. To elucidate the magnetic orbital interactions, natural orbital analysis (NO analysis) is performed. For the magnetostructural correlations, simplest Ni models are employed and the magnetic interactions are analyzed theoretically.

* Corresponding author. E-mail: mshoji@chem.sci.osaka-u.ac.jp.

10.1021/jp711525q CCC: $40.75
Published on Web 04/05/2008

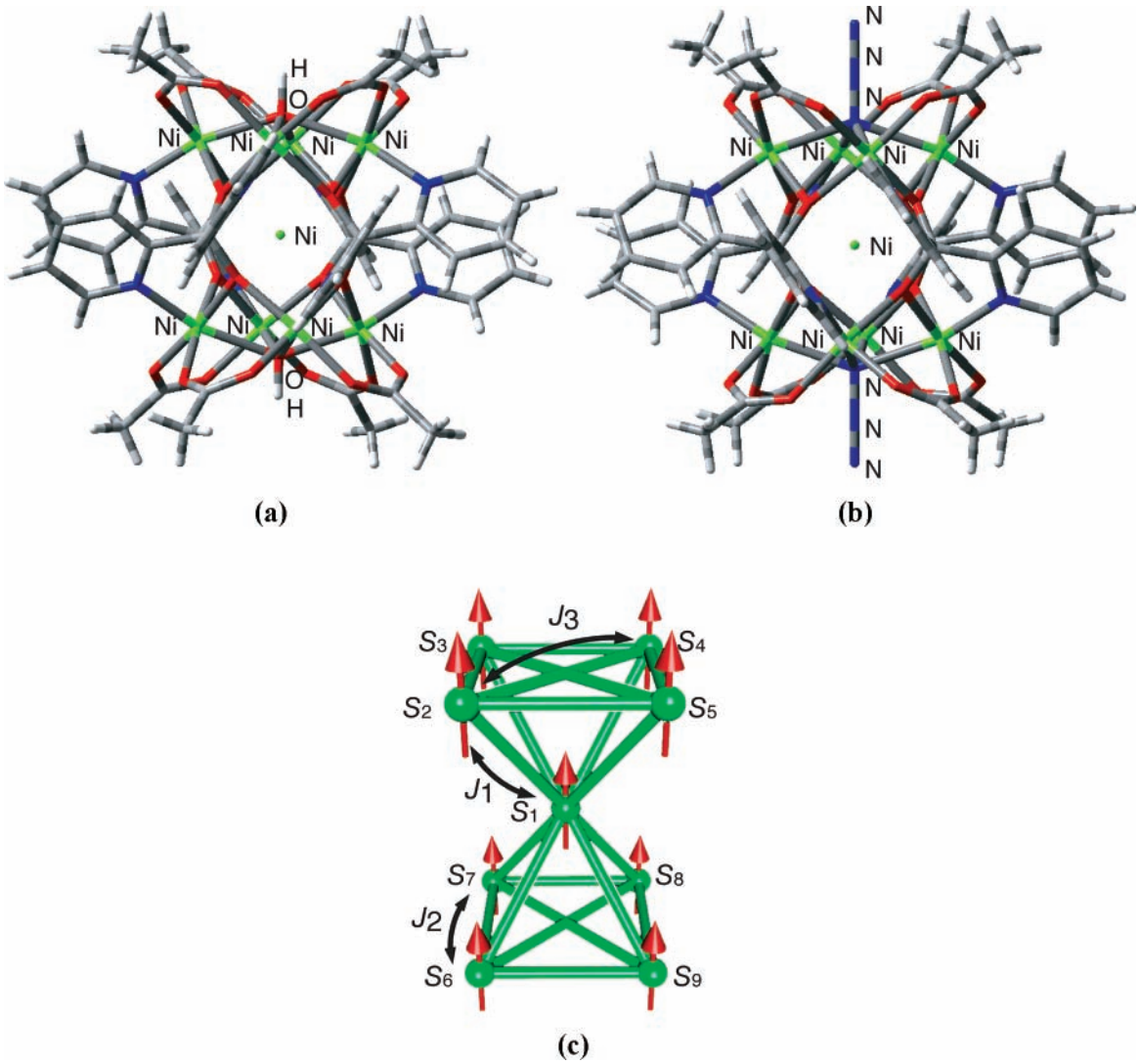

Figure 1. Molecular structures of the Ni_9 complexes $Ni_9L_2(O_2CMe)_8\{(2\text{-py})_2CO_2\}_4$, (a) L = OH (**1**) and (b) L = N_3^- (**2**), used in this study. Atoms are colored using the following scheme: Ni, green; N, blue; O, red; C, gray, H, white. (c) Spin structure of the Ni_9 complex. Arrows schematically denote the spins at the Ni sites.

2. Theoretical Background

2.1. Spin Hamiltonian and Effective Exchange Integral (*J*). The magnetic cage of the Ni_9 consisted of a central Ni(II) and eight Ni atoms in two square planes, forming two square pyramids linked at the top positions (Figure 1c). The cage has three different superexchange pathways: J_1, J_2, and J_3. J_1 is a magnetic interaction through a μ-O of the di-2-pyridyl ketone ligand: $(2\text{-py})_2CO_2^{2-}$. J_2 is a magnetic interaction through a carboxylate group of an acetic acid ligand. J_3 is a magnetic interaction through the terminal ligand L, which is a hydroxyl or an azido anion for **1** or **2**, respectively. All Ni atoms are octahedrally coordinated by ligand atoms.

The spin Hamiltonian of the Ni_9 cage is defined by

$$H = -2J_1(\mathbf{S}_1\cdot\mathbf{S}_2 + \mathbf{S}_1\cdot\mathbf{S}_3 + \mathbf{S}_1\cdot\mathbf{S}_4 + \mathbf{S}_1\cdot\mathbf{S}_5 + \mathbf{S}_1\cdot\mathbf{S}_6 + \mathbf{S}_1\cdot\mathbf{S}_7 + \mathbf{S}_1\cdot\mathbf{S}_8 + \mathbf{S}_1\cdot\mathbf{S}_9) - 2J_2(\mathbf{S}_2\cdot\mathbf{S}_3 + \mathbf{S}_3\cdot\mathbf{S}_4 + \mathbf{S}_4\cdot\mathbf{S}_5 + \mathbf{S}_5\cdot\mathbf{S}_2 + \mathbf{S}_6\cdot\mathbf{S}_7 + \mathbf{S}_7\cdot\mathbf{S}_8 + \mathbf{S}_8\cdot\mathbf{S}_9 + \mathbf{S}_9\cdot\mathbf{S}_6) - 2J_3(\mathbf{S}_2\cdot\mathbf{S}_4 + \mathbf{S}_3\cdot\mathbf{S}_5 + \mathbf{S}_6\cdot\mathbf{S}_8 + \mathbf{S}_7\cdot\mathbf{S}_9) \quad (1)$$

where $\mathbf{S}_i$ is the *i*th Ni spin site ($S = 1$). $\mathbf{S}_1$ is the central Ni spin and the other spins, $\mathbf{S}_{2-9}$, are at the square corners. Though the magnetic anisotropy will be considerably important at the large-spin states, the isotropic magnetic interactions are focused in this study.

Four Ising spin states were calculated for the Ni_9s using the broken-symmetry (BS) method. The Ising spin (=BS) states are summarized in Table 1. From the eq 1, total energies at the BS states are given as follows,

$$E_1 = -16J_1 - 16J_2 - 8J_3$$
$$E_2 = 16J_1 - 16J_2 - 8J_3$$
$$E_3 = 16J_2 - 8J_3$$
$$E_4 = 8J_3 \quad (2)$$

where E_i denotes the total energy at the BS spin state *i*. Applying the energy levels to first principle BS results, the *J* values can be evaluated by solving the above linear equations.

For two-spin site systems, the approximate spin projection (AP) procedure can be used to calculate the Heisenberg *J* value,[10,11] which is given by

$$J_{ab}^{AP} = \frac{^{LS}E_X - ^{HS}E_X}{^{HS}\langle S^2\rangle_X - ^{LS}\langle S^2\rangle_X} \quad (3)$$

where $^{Y}E_X$ and $^{Y}\langle S^2\rangle_X$ are the total energy and the total squared-magnitude of spin state Y by method X (X = UHF, UHDFT, CASSCF), respectively. In the AP method, orbital overlaps between the spin orbitals are considered. For multinuclear spin systems, the generalized spin procedure (GP) can be applied to evaluate the Heisenberg J values.[12] On the other hand, eq 2 neglects the orbital overlaps; therefore, the J values evaluated by eq 2 are denoted as Ising J values. Fortunately for Ni_9 complexes, the Ising treatment is sufficiently reliable, because the overlaps are negligibly small. In fact, the differences between the calculated Ising and Heisenberg J values are less than 1 cm^{-1}.[12]

2.2. Natural Orbital Analysis. Natural orbitals φ_i are obtained by diagonalization of a charge density matrix (first-order reduced density matrix), which is written as

$$\rho(x,x') = \sum_i n_i \varphi_i(x)\, \varphi_i(x') \quad (4)$$

where n_i is the occupation number of the ith natural orbital φ_i. At the BS spin state (antiferromagnetically coupled spin state), the natural orbitals with fractional occupations (FNO's) represent the spin orbitals.[13,14] On the basis of the occupation numbers, the FNO's are classified as higher occupied natural orbitals (HONO's) and lower unoccupied natural orbitals (LUNO's). The HONO's and LUNO's are formed in pairs at the BS spin state of the two spin sites systems. These FNO's are clearly divided into interaction types of the spin orbitals. From the occupation numbers, characteristic chemical indices such as T, b, I, Q, U, Y, and B values can be derived.[5,6,15] These chemical indices are useful to analyze the electron correlation effects and to characterize the chemical bonds. Here, the T value is mainly used to characterize the magnetic interactions.

Spin-polarized orbitals of BS solutions, ϕ_α and ϕ_β, are related to natural orbitals and occupation numbers as

$$\varphi_\pm = \frac{1}{\sqrt{2(1 \pm T)}}(\phi_\alpha \pm \phi_\beta) \quad (5a)$$

$$n_\pm = 1 \pm T \quad (5b)$$

where $\varphi_+(\varphi_-)$ is the (anti)bonding natural orbital and $n_+(n_-)$ is the occupation number. The T value is an orbital overlap integral between the α and β spin-polarized orbitals, ϕ_α and ϕ_β. It should be noted that the T value is equal to a bond order b. Thus T and b values can be evaluated by the difference between the occupation numbers of bonding and antibonding natural orbitals, i.e., HONO's and LUNO's, as

$$T = \frac{n_+ - n_-}{2} = b \quad (6)$$

For example, if the T value is 1.0, the bond is in a completely closed-shell (b = 1.0), and if the T value is 0.0, the bond is completely broken and is in a diradical state (b = 0).

3. Computational Procedures

All calculations were performed with the Gaussian98 program package.[16] The B3LYP functional was used for hybrid density functional (HDFT) calculations.[17−19] Effective core potentials, CEP-31G basis sets, were used for full model (**1**, **2**) calculations.[20−22] All position coordinates of **1** and **2** were taken from the X-ray structure data in the Cambridge Structural Database (CSD).[23] The CSD codes were ACOFIH and ACOFON for **1** and **2**, respectively.[8] To investigate each magnetic interaction pathway, apomodels were also used, where unnecessary Ni atoms were replaced by point charges (2+). Simplified models (**3**, **4**) composed of two Ni atoms and bridging ligands were used to investigate the correlation between the magnetic interactions and the geometrical parameters at the dinuclear sites. Substitute point charges (−0.5) were used for the terminal ligands. The distance between the Ni center and the point charge was kept at 2.1 Å. Huzinaga MIDI basis and Hay's diffuse basis sets were used for the Ni atom, and 6-31G* basis sets were used for the others in **3** and **4**.[24−27] These all-electron basis sets are double-ζ plus polarization (DZP) quality.

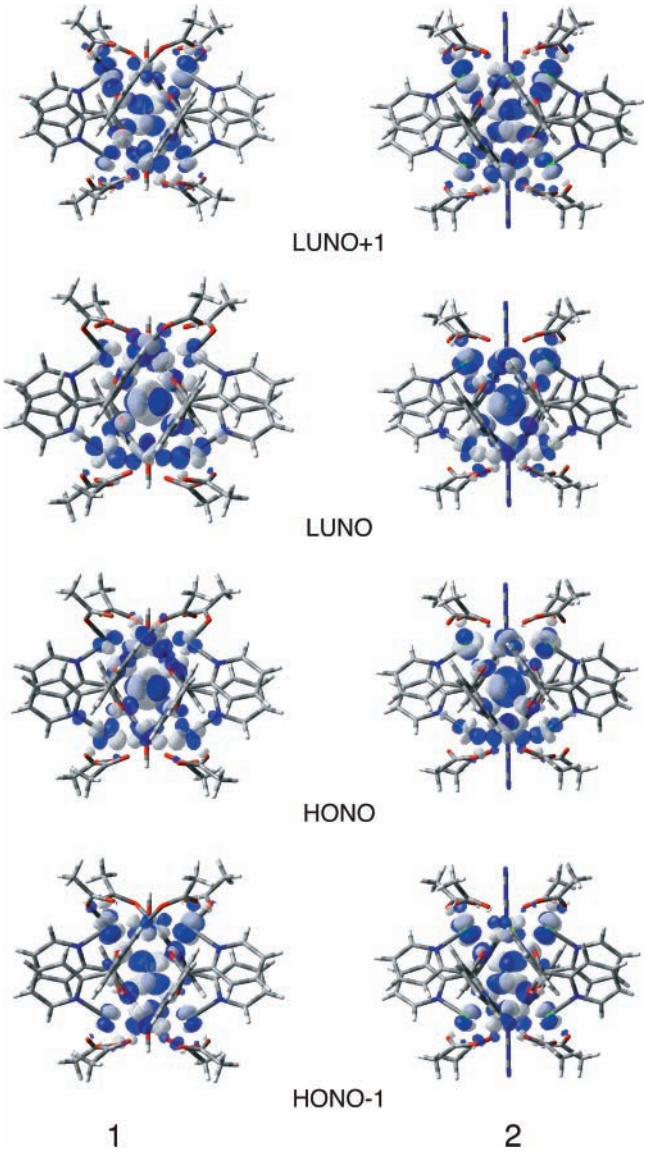

Figure 2. Natural orbitals (NO) of the J_1 exchange interactions in the Ni_9 complexes: (left) **1** and (right) **2**. These NO's are computed from the UB3LYP/DZP method at the spin state 2 of the Ni_9 full models.

4. Results and Discussion

4.1. Magnetic Orbital Interactions of 1 and 2. Full model calculations were performed at the B3LYP/CEP-31G level. Four BS spin states were calculated for each Ni_9 complex (Table 1). The J values for the full models from eq 2 were J_1 = 4.5 cm^{-1},

TABLE 2: Calculated Interaction Types and the Orbital Overlap Integral (*T* Value[a]) for Each Magnetic Interaction in the Ni_9 Complexes

		T_I					
		$I = J_1$		$I = J_2$		$I = J_3$	
molecule	NO						
1	HONO−1 LUNO+1	$d_{x^2-y^2}$	0.0590	mix[b]	0.0223	σ	0.0746
	HONO LUNO	d_{z^2}	0.0182	mix[b]	0.0151	δ	0.0076
2	HONO−1 LUNO+1	$d_{x^2-y^2}$	0.0651	mix[b]	0.0285	σ	0.0514
	HONO LUNO	d_{z^2}	0.0177	mix[b]	0.0190	δ	0.0123

[a] *T* values are calculated by full- and apo-models at the UB3LYP/ECP-31G level. [b] Mixture of the $\sigma-\sigma$ and $\delta-\delta$ interactions.

$J_2 = 5.5\ cm^{-1}$, and $J_3 = -29.3\ cm^{-1}$ for **1** and $J_1 = 4.4\ cm^{-1}$, $J_2 = 6.3\ cm^{-1}$, and $J_3 = 0.7\ cm^{-1}$ for **2**.[9] It is clearly shown that the essential difference is only J_3 interaction. These values are comparable to the experimentally determined *J* values, $J_1 = 3.0\ cm^{-1}$, $J_2 = 9.0\ cm^{-1}$, and $J_3 = -28.5\ cm^{-1}$ for **1**, which were evaluated from the temperature-dependent magnetic susceptibility curve.[8]

Magnetic interactions of the J_1 pathways are discussed using the natural orbitals (NO's). In Figure 2, the orbital interactions between the central Ni spin and the other surrounding eight spin sites are shown. These NO's are evaluated by the UB3LYP calculation at the spin state 2 of the full models. The HONO and LUNO are characterized as orbital interactions between the d_{z^2} type orbitals in the central Ni and other d orbitals in the surrounding Ni, because the HONO and LUNO are different only at the node of the central d_{z^2} orbitals. On the other hand, the HONO−1 and LUNO+1 show another J_1 magnetic interactions between the $d_{x^2-y^2}$ orbitals in the central Ni center and other d orbitals in the surrounding Ni. From the *T* values of these interactions, it can be concluded that the latter interactions ($d_{x^2-y^2}$) have relatively stronger overlaps than the former (d_{z^2}). The *T* values for **1** are 0.059 and 0.0182, respectively. The *T* values are listed in Table 2. The shapes of the NO's and the *T* values are similar for **1** and **2**. In fact, these orbital interactions are not related to the bridging ligand L.

To investigate the magnetic interactions between the Ni spin sites, apomodels are employed, where unnecessary Ni atoms in other interaction pathways are replaced by point charges, because it is inevitable that all magnetic interactions of multinuclear metal complexes will be mixed in the natural orbitals at the BS spin states. For the Ni_9 cage, the J_2 and J_3 magnetic interactions mix at the BS states 3 and 4, and it is impossible to analyze individual magnetic interactions from the natural orbital analysis. In the apomodel 2 (**A2**), all Ni atoms except for those at S_2 and S_3 positions are replaced by point charges. In the apomodel 3 (**A3**), all Ni atoms except for those at S_2 and S_4 positions are replaced by point charges. Using these apomodels (**A2**, **A3**), the magnetic interactions of J_2 and J_3 are investigated.

From the apomodels, *J* values are calculated by following the AP procedure (eq 3). They are $J_2 = 4.81\ cm^{-1}$ and $J_3 = -29.41\ cm^{-1}$ for **1** and $J_2 = 6.50\ cm^{-1}$ and $J_3 = -0.54\ cm^{-1}$ for **2** by the UB3LYP method. These results are in reasonable agreement with the full model results. Because the point charge substitution of unnecessary Ni atoms is a quite drastic approximation, the magnetic orbitals are localizing over the Ni spin centers and mediating ligands. Thus the approximation is appropriate for these Ni complexes. It is shown that these apomodels are appropriate to investigate the magnetic interactions.

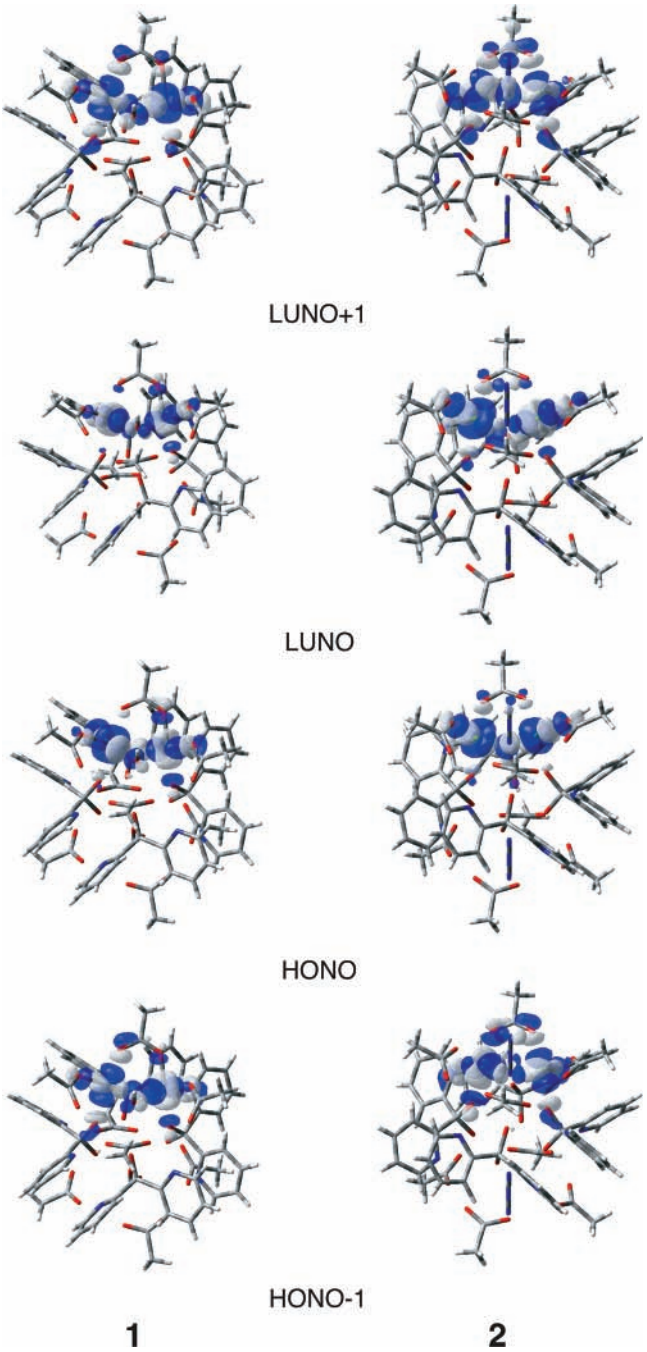

Figure 3. Natural orbitals (NO) of the J_2 exchange interactions in the Ni_9 complexes: (left) **1** and (right) **2**. These NO's are computed from the UB3LYP/DZP method at the antiferromagnetic spin state of the Ni_9 apo-models (apomodel 2).

Figure 3 shows the magnetic interactions between the neighboring Ni spins at the square pyramid base, which correspond to the J_2 interaction pathways. These NO's are calculated using **A2** and are a mixture of d_{z^2} and $d_{x^2-y^2}$ type orbitals. The *T* values for **1** are 0.0223 and 0.0151, respectively, and are relatively small. These small *T* values are reasonable because J_2 is a ferromagnetic interaction ($J_2 > 0$) and the Ni−ligand−Ni angles are almost orthogonal. Almost the same features are observed for **2**: the NO's and the *T* values of **2** are similar to those of **1**.

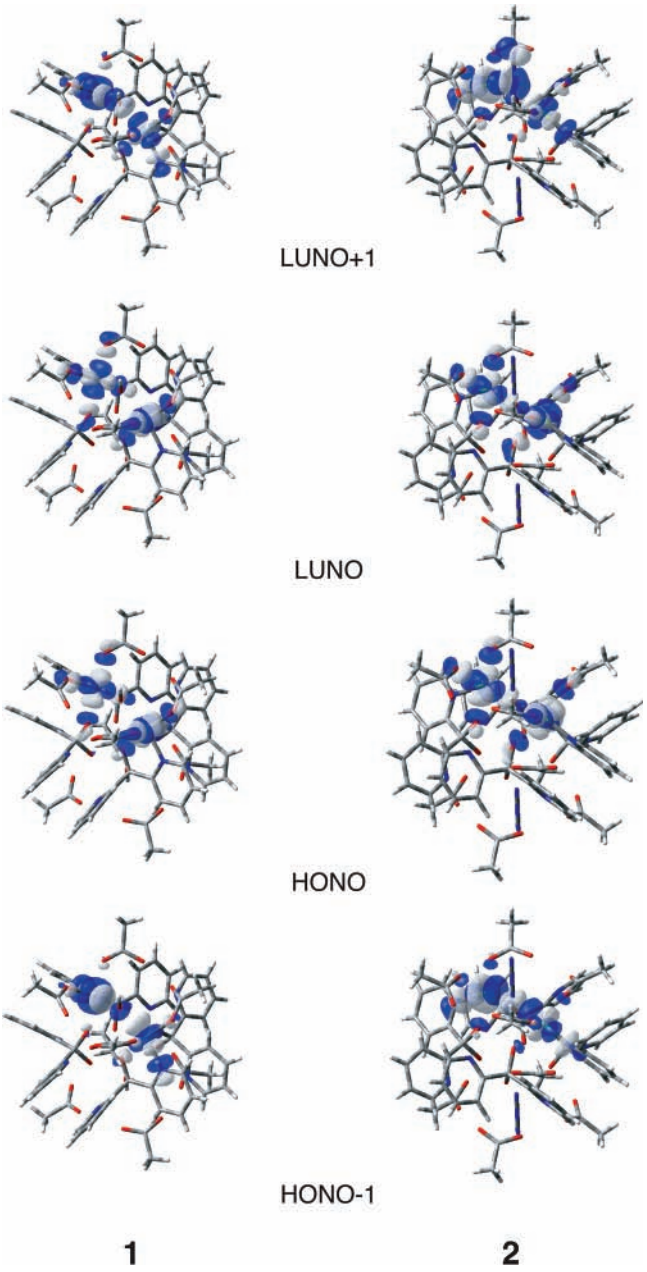

Figure 4. Natural orbitals (NO) of the J_3 exchange interactions in the Ni_9 complexes: (left) **1** and (right) **2**. These NO's are computed from the UB3LYP/DZP method at the antiferromagnetic spin state of the Ni_9 apo-models (apomodel 3).

The NO's for the J_3 interaction pathways are calculated using **A3**, and are shown in Figure 4. These NO's are assigned to the σ and δ type interactions. The HONO−1 and LUNO+1 indicate the σ-interaction between the d_{z^2} type Ni orbitals through the bridging ligand L. The HONO and LUNO are characterized as the δ interaction between the $d_{x^2-y^2}$ type Ni orbitals. The T values of **1** are 0.0746 and 0.0076 for σ and δ interactions, respectively. It is noteworthy that the σ interactions have larger orbital overlaps. On the other hand, for **2**, the T values are 0.0514 and 0.0123, respectively. The main σ interactions of the azido ligands are suppressed. This result is in accord with the drastic decrease in the antiferromagnetic J_3 couplings (J_3 values).

If the J_3 antiferromagnetic interaction is dominant ($J_3 \leq = -7.6\ cm^{-1}$),[9] the ground spin state of Ni_9 complex becomes $S = 1$. At this $S = 1$ state, spin correlation functions for J_1, J_2 and J_3 interactions are $\langle S_1 \cdot S_{i\neq 1}\rangle = 0$, $\langle S_{i\neq 1} \cdot S_{i+1}\rangle = 0$ and $\langle S_{i\neq 1} \cdot S_{i+2}\rangle = -2$, respectively. For the local spin densities, only the central spin takes a nonzero value, $\mathbf{S}_1 = 1$, $\mathbf{S}_i = 0$ ($i = 2-9$). The surrounding spins, $\mathbf{S}_i$, ($i = 2-9$), are singlet-coupled for the J_3 interactions, and the local spin momentums are canceled out each other. Thus the J_3 interaction is significantly important for the magnetism of the Ni_9 complexes.

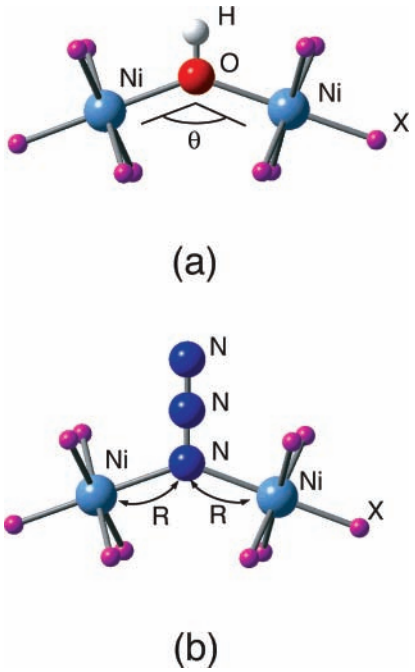

Figure 5. Simplified models used in this study. Binuclear Ni(II) atoms are bridged by ligands L and the other terminal ligands are substituted by point charges (X). (a) $L = OH^-$ (**3**) and (b) $L = N_3^-$ (**4**). The geometrical variables are bridging angle (θ) and ligand−metal bond length (R). Atoms are colored using the following scheme: Ni, light blue; N, blue; O, red; H, white; X, violet.

In the next section, validity of the calculated J_3 values for the Ni_9 complexes are discussed by investigating the magnetostructural correlations, comparing to other synthesized Ni complexes.

4.2. Correlation between the Exchange Integral (J) and the Core Geometry. The magnetostructural correlations between the J values and the geometrical parameters of the Ni cores have been reported previously. On the basis of a number of azido−bridged Ni complexes, Ribas and co-workers reported that the Ni−N_3−Ni angle θ is in the range 101−104° and that they are ferromagnetic couplings from 30 to 40 cm^{-1}.[28−36] The Ni−N bond lengths are in the range of 2.0−2.3 Å. Ruiz reported the θ dependence of the J value by DFT calculations using model complexes.[37] Compared to these dinuclear Ni azido complexes, the geometrical parameters of **2** are outside the range, where the Ni−N bond length and Ni−N−Ni angle are 2.3 Å and 142°, respectively. The J value dependence of these geometrical ranges and magnetic interactions has not yet been studied. In this study, a theoretical investigation of the magnetic interactions is conducted.

The molecular structures of the simplified models **3** and **4** are shown in Figure 5a and 5b, respectively. The bond angles θ are varied from 100° to 180° with the bond lengths (R) held at 2.0, 2.2 and 2.4 Å. Following the AP procedure of eq 3, the J values are evaluated. The calculated J curves are presented in Figure 6a,b for **3** and **4**, respectively. These curves suggest that the magnetic interactions are significantly affected by θ and R. As the θ value increases, both **3** and **4** increase the

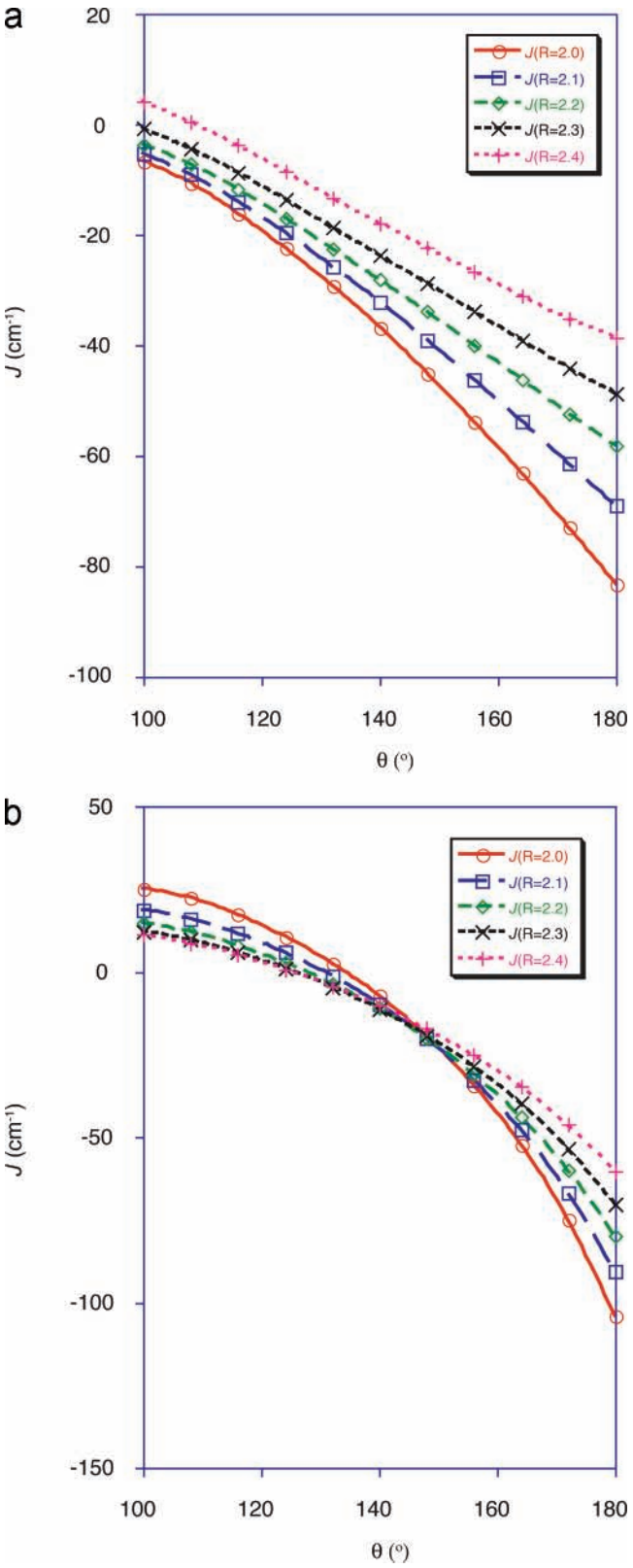

Figure 6. Calculated J values of simplified models: (a) **3 (**simplified model of L = OH^-**)** and (b) **4 (**simplified model of L = N_3^-**)** by the UB3LYP/DZP method as a function of the Ni−O−Ni bridging angle (θ).

antiferromagnetic interactions. On the other hand, as the R value increases, the antiferromagnetic interactions are suppressed. For **3**, the weak antiferromagnetic interaction at $\theta = 100°$ is turned to weak ferromagnetic interactions and stronger antiferromagnetic interaction at $\theta = 180°$ is drastically decreased. For **4**, the R value decreased the magnetic interactions. At $\theta = 100°$ the ferromagnetic interaction is decreased, and at $\theta = 180°$ the stronger antiferromagnetic interaction is decreased by half.

For the hydroxyl model **3**, J is an antiferromagnetic interaction for the whole θ region, except for a small region at $\theta = 90°$ and $R = 2.4$ Å. Magnetic measurements of hydroxyl bridged Ni complexes were reported to show weak antiferromagnetic interactions.[38] The reported J value for $[Ni_2(\mu\text{-OH})(\mu\text{-}CH_3CO_2)_2L_2]ClO_4$ is -4.5 cm^{-1}, where θ and R are 115.1° and 2.0 Å, respectively.[39] The calculated J value of **3** at $\theta = 116°$ and $R = 2.0$ Å is -16.12 cm^{-1}. For **1,** the calculated J_3 value was -29.3 cm^{-1} and the fitted J value to the experimental magnetic susceptibility curve was -28.5 cm^{-1},[8] which are compared with the calculated -23.68 cm^{-1} of **3** at $\theta = 140°$ and $R = 2.3$ Å.

For the azido model **4**, calculated J values are 25.18, 18.78, 14.72, and 11.15 cm^{-1} at $\theta = 100°$ for $R = 2.0$ Å, $R = 2.2$ Å, and $R = 2.4$ Å, respectively. These calculated J values are comparable to the experimental values: ($J = 26.9$ cm^{-1}, $\theta = 103.8°$, $R = 2.08$ Å) of $[Ni_2Me_3[12]N_3]_2(\mu\text{-}N_3)_2](ClO_4)_2$, ($J = 26.8$ cm^{-1}, $\theta = 104.3°$, $R = 2.13$ Å) of $[Ni_2en_4(\mu\text{-}N_3)_2](ClO_4)_2$, and ($J = 16.9$ cm^{-1}, $\theta = 104.9°$, $R = 2.17$ Å) of $[Ni_2(232\text{-}N_4)_2(\mu\text{-}N_3)_2](ClO_4)_2$.[28−30] It should be noted that the ferromagnetic interaction of the azido bridge exists only below $\theta = 140°$. From the simple model **4**, the calculated J value for the J_3 interaction of **2** is $J = -11.23$ cm^{-1} (at $\theta = 140.0°$, $R = 2.3$ Å), where the estimated J value by fitting the experimental χT curve is $J = -9.0$ cm^{-1}.[9] Compared to these J values, the J_3 value of the full model is rather small. Ruiz et al. have reported that effective core potentials tend to underestimate antiferromagnetic contributions relative to all electron basis sets.[40]

Figure 7 shows four NO's of **3** and **4**. We can see two pairs of HONO's and LUNO's. The HONO−1 and LUNO+1 pair corresponds to a σ-type interaction between the d_{z^2} orbitals of the Ni atoms. The HONO and LUNO pair corresponds to a δ-type interaction between the $d_{X^2-Y^2}$ orbitals of the Ni atoms. These NO's of **3** and **4** are very similar to those of the J_3 interactions of **1** and **2** (Figure 4), respectively. The shapes of HONO−1 and LUNO+1 are noticeable. The mediating orbitals of the bridging ligands are p and π orbitals of OH^- and N_3^-, respectively, which corresponds to HOMO orbitals of the ligand fragments. In fact, if the LUNO+1s are projected to the ligand flagment orbitals, largest coefficients are seen for the ligand HOMO's, the coefficients are 0.356 and 0.375 for **3** and **4**, respectively at $\theta = 140.0°$, $R = 2.3$ Å. On the other hand for the HONO−1s, major parts are from their inner orbitals, ligand HOMO−3's, the coefficients are 0.106 and 0.127 for **3** and **4**, respectively. These NO's clearly show us what is the most important ligand orbital for each magnetic interaction (Figure 4). It is noted that the LUNO+1s have similar shapes to ligand to metal charge transfer orbitals (LMCT). It is also noteworthy that these HOMO−LUNO pairs are spin delocalization (SD) orbitals, which can be observed by experiments. For Cu azido complexes, spin polarizations at azido ligand were observed by neutron scattering.[41] The spin polarization densities are very similar in shape to the NO's shown in the Figure 4.

The occupation numbers of the NO's are related to the orbital overlap (T) as defined in eq 5. The θ dependences of the T values of **3** and **4** are shown in Figure 8. The T values of the δ interactions are almost zero, indicating that the orbital interactions are significantly weak. On the other hand, the T values of the σ-type interactions are larger, indicating that the main magnetic pathways between the Ni atoms are the σ-type interactions. As θ decreases from 180°, the T values gradually decrease for both **3** and **4**. At $\theta = 180°$ and $R = 2.0$ Å, the T

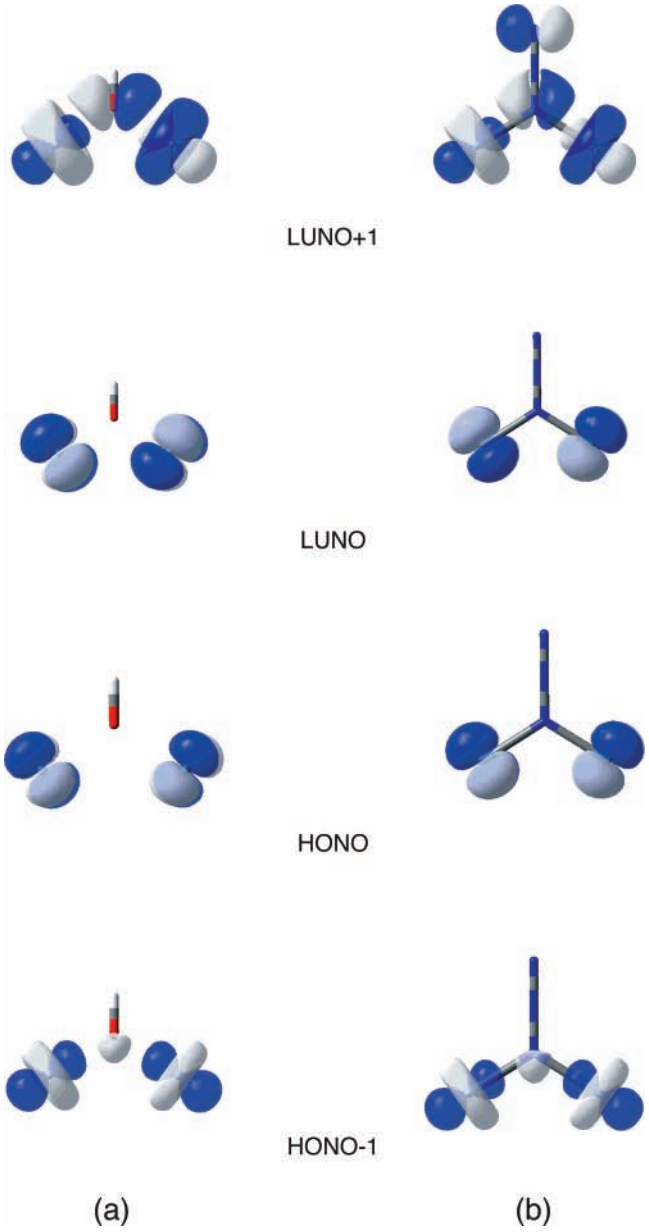

Figure 7. Natural orbitals (NO) of the exchange interactions in the simplified models, (a) **3** and (b) **4**. These NO's are calculated by the UB3LYP/DZP method at the antiferromagnetic spin states.

values are 0.138 and 0.182 for **3** and **4**, respectively, and are 0.073 and 0.055 at $\theta = 100°$. These T values at $\theta = 100°$ are comparable with those in the full models, $T = 0.0746$ and 0.0514, respectively. The azido ligand (**4**) has a higher T value than the hydroxyl one (**3**). Therefore, we can conclude that the ferromagnetic interaction of the azido ligands can be attributed to the orthogonality of the spin orbitals, where the main σ-type antiferromagnetic interaction is suppressed at around $\theta = 100°$ due to the orthogonality.

It is noted that the R parameter is not a significant factor for T values.

4.3. Relationship between the Effective Exchange Integral (J) and Spin Orbital Overlap Integral (T). The results of the model systems, **3** and **4** show the strong correlations between the effective exchange integral (J value) and the orbital overlap (T value): as the T value increases, the interaction strengthen the antiferromagnetic coupling. This correlation is commonly observed for other correlated spin systems. This rule can be explained in terms of the Hubbard model, which is widely used

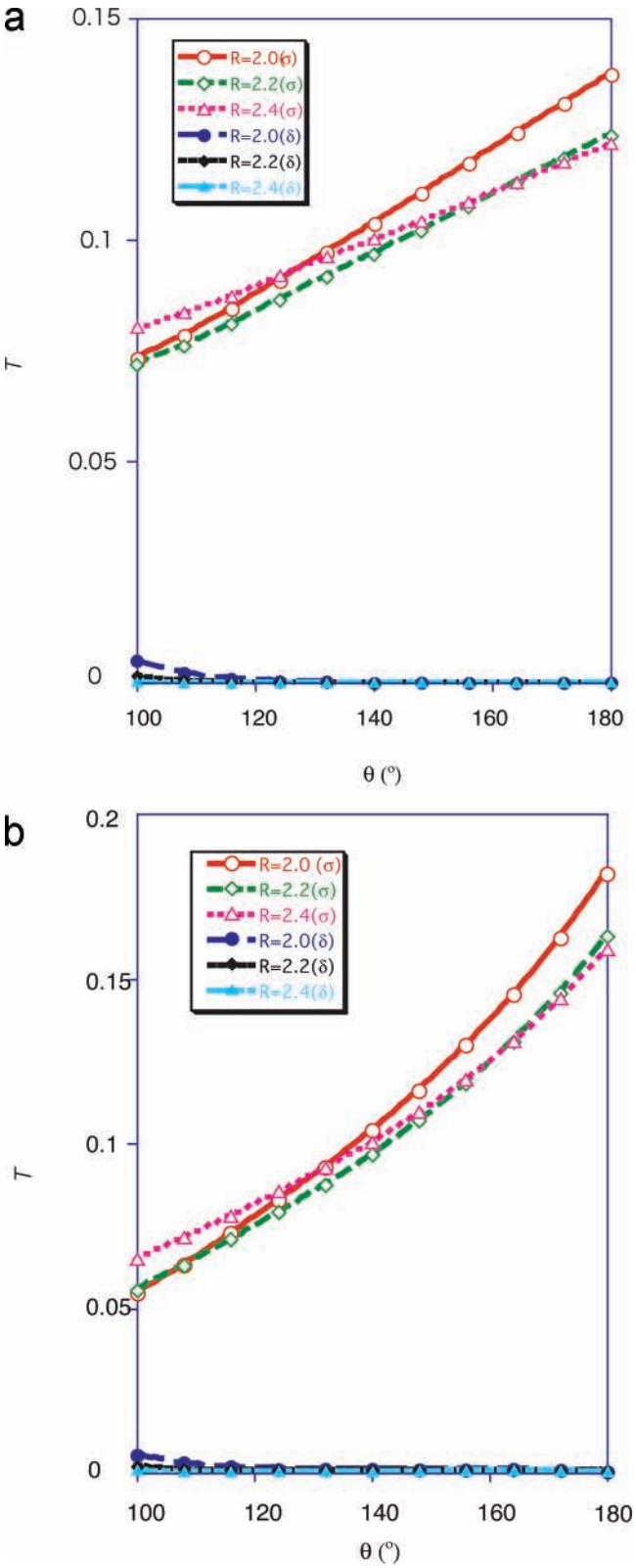

Figure 8. Spin orbital overlap (T) dependences as a function of the bridging angle (θ) in the simplified models: (a) L = OH^- and (b) L = N_3^-. These T values are calculated by the UB3LYP/DZP method at the antiferromagnetic spin states.

in the solid-state physics to describe the magnetic phases. The Hubbard Hamiltonian is expressed as

$$H = -\sum_{i,j\neq i}\sum_{\sigma} t_{ij} a^{\dagger}_{i,\sigma} a_{i,\sigma} + \frac{1}{2}\sum_{k} U_k a^{\dagger}_{k,\alpha} a_{k,\alpha} a^{\dagger}_{k,\beta} a_{k,\beta} \qquad (7)$$

TABLE 3: Calculated Effective on-Site Columbic Integral *U* in the Dinuclear Ni Models, 3 and 4

	U/eV		
model	$R = 2.0$	$R = 2.2$	$R = 2.4$
3	5.78	5.52	5.23
4	4.43	4.20	3.54

where t and U are a transfer integral and an on-site coulomb integrals. The subscript i, j, and k indicate Ni spin sites. The Hubbard Hamiltonian can be converted to the Heisenberg model such as eq 1 at the strong correlation limit: $t/U \ll 1$. According to the Kahn's scheme, the effective exchange interaction can be decomposed as a sum of ferromagnetic (J_F) and antiferromagnetic (J_{AF}) contributions.[42] Using the Hubbard model of a simple two electrons two sites model, the J_{AF} contribution can be expressed as follows,

$$\begin{aligned} J &= J_F + J_{AF} \\ &= J_F + \frac{U}{4}(1 - \sqrt{1 + 4T^2}) \\ &\approx J_{T=0} - \frac{U}{2}T \end{aligned} \tag{8}$$

where $J_{T=0}$ is a J value at $T = 0$ (for details, see Supporting Information). The t value is given by

$$t = \frac{U}{2}T \tag{9}$$

As can be seen from eq 8, the T value is linearly dependent on the J value, because the U value is approximately constant for homo multinuclear metal centers. This Hubbard model has more parameters than the Heisenberg model, a careful treatment for the parameters such as t, $J_{T=0}$ and U, is mandatory for the applications for multinuclear spin systems. For a system of dinuclear Ni ($S = 1$) spins, the eq 8 can be expanded as

$$\begin{aligned} E_{S=2} - E_{S=0} &= -6J \\ &= -\frac{3}{2}J_\sigma \\ &= \frac{3}{4}E_G \\ &= -\frac{3}{2}J_{T=0} - \frac{3U}{8}(1 - \sqrt{1 + 4T_\sigma^2}) \end{aligned} \tag{10}$$

under the assumption that the magnetic interaction is occurred through one (σ-type) interaction. The eq 10 well reproduced the correlations between the J and T values of **3** and **4** (see Supporting Information). From the slope of the lines, the effective U value of the Ni centers can be determined as $U = 5.23$ eV and $U = 3.54$ eV at $R = 2.4$ Å for **3** and **4**, respectively. Calculated U values are summarized in Table 3. These large U values indicate the characteristic feature of the strong correlation of the Ni centers. As the R value increase, the U value decreases gradually for the change of the geometrical core structures.

5. Conclusions

The magnetic interactions, J values, and the overlap integrals, T values, of the Ni_9 complexes have been investigated using density functional theory calculations. Using apomodels, each individual magnetic interaction was depicted by natural orbital analysis. The calculated J values of the apomodels are consistent with the results of the full models. Both Ni_9 complexes (L = OH^- and L = N_3^-) have almost the same J_1 and J_2 values, and the J_3 values are different. J_3 is the superexchange interaction through the bridging ligands L. It is concluded that the magnetic properties of the Ni_9 complexes are changed by the J_3 interaction. NO's for the J_3 interaction pathway clearly showed that the main interaction is σ-type and is composed of d_{z^2} orbitals at the Ni centers and p and π orbitals of the bridging ligand OH^- and N_3^-, respectively.

Using simplified models, the structure dependences of the magnetic interactions of the OH^- and N_3^- were examined. The J values calculated from these simplified models were qualitatively reproduced not only for the results of the inorganic complexes but also for the Ni_9 complexes. The J values strongly depended on the geometrical parameters: Ni−L−Ni angle θ and Ni−L bond length. As θ decreases from 180° to 100°, the magnetic interactions reduced the antiferromagnetic couplings for both ligands. The Ni−L bond length reduced the magnitude of the magnetic interactions. It was observed that the J values and the orbital overlap (T) values correlate with each other. Using the Hubbard model, the relationship between the J values and T values is clarified. The results of simplified models clearly show that the major difference of the magnetic properties between the OH^- and N_3^- ligands is attributed for the orbital overlap interaction (T value). Thus, the ferromagnetic couplings of the azido ligand seen in dinuclear Ni inorganic complexes are attributed to the orthogonality of the spin orbitals. For the azido ligand, the ferromagnetic interaction can exist in the case of $\theta < 113°$ at $R = 2.3$ Å. From the structural parameters of $\theta = 142°$ and $R = 2.3$ Å of **2**, a weak antiferromagnetic interaction is appropriate for **2**. The weak antiferromagnetic interaction of the azido ligand of **2** is attributed to the unusually large bond angle, which are constrained by the four $(2\text{-py})_2CO_2^{2-}$ ligands.

Acknowledgment. M.S. is grateful for the financial support (Research Fellowships) from the Japan Society for the Promotion of Science (JSPS) for Young Scientists. This work has been supported by the Grants-in-Aid for Scientific Researches (KAKENHI 19750046, 19350070, 18350008) from JSPS and that on the Priority Area (19029028) from the Ministry of Education, Culture, Sports, Science and Technology (MEXT).

Supporting Information Available: Tables of J values for **1** and **2** (Table S1); chemical indices for the magnetic interactions of **1** and **2** (Table S2 and S3); bridging angle θ dependence of the J and T values for **3** and **4** (Table S4 and S5); figures of the correlation between the J values and T values for **3** and **4** (Figure S1); Table of the fitting parameters of the correlation lines (Table S6); detailed explanations for the "notation of the chemical indices" and the "derivation of the Hubbard model representation". This material is available free of charge via the Internet at http://pubs.acs.org.

References and Notes

(1) Sessoli, R.; Gatteschi, D.; Caneschi, A.; Novak, M. A. *Nature* **1993**, *365*, 141.

(2) Thomas, L.; Lionti, F.; Ballou, R.; Gatteschi, D.; Sessoli, R.; Barbara, B. *Nature* **1996**, *383*, 145.

(3) Wernsdorfer, W. *Adv. Chem. Phys.* **2001**, *118*, 99.

(4) Shoji, M.; Koizumi, K.; Hamamoto, T.; Taniguchi, T.; Takeda, R.; Kitagawa, Y.; Kawakami, T.; Okumura, M.; Yamanaka, S.; Yamaguchi, K. *Polyhedron* **2005**, *24*, 2708.

(5) Shoji, M.; Nishiyama, Y.; Maruno, Y.; Koizumi, K.; Kitagawa, Y.; Yamanaka, S.; Kawakami, T.; Okumura, M.; Yamaguchi, K. *Int. J. Quantum Chem.* **2004**, *100* (6), 887.

(6) Shoji, M.; Hamamoto, T.; Koizumi, K.; Isobe, H.; Kitagawa, Y.; Takano, Y.; Yamanaka, S.; Yamaguchi, K. *Polyhedron* **2005**, *24*, 2701.

(7) Shoji, M.; Koizumi, K.; Kitagawa, Y.; Yamanaka, S.; Kawakami, T.; Okumura, M.; Yamaguchi, K. *Int. J. Quantum Chem.* **2005**, *105*, 628.
(8) Papaefstathiou, G. S.; Escuer, A.; Vicente, R.; Font-Bardia, M.; Solans, X.; Perlepes, S. P. *Chem. Commun.* **2001**, 2414.
(9) Shoji, M.; Koizumi, K.; Hamamoto. T.; Kitagawa, Y.; Yamanaka, S.; Okumura, M.; Yamaguchi, K. *Chem. Phys. Lett.* **2006**, *421*, 483.
(10) Yamaguchi, K.; Takahara, Y.; Fueno, T. In *Applied Quantum Chemistry*; Smith, V. H., Jr., Scheafer, H. F., III, Morokuma, K., Eds.; D. Reidel: Boston, 1986; p 155.
(11) Yamaguchi, K.; Fukui. H.; Fueno, T. *Chem. Lett.* **1986**, 625.
(12) Shoji, M.; Koizumi, K.; Kitagawa, Y.; Kawakami, T.; Yamanaka, S.; Okumura, M.; Yamaguchi, K. *Chem. Phys. Lett.* **2006**, *432*, 343.
(13) Yamaguchi, K. *Chem. Phys. Lett.* **1975**, *33*, 330.
(14) Takano, Y.; Kitagawa, Y.; Onishi, T.; Yoshioka, Y.; Yamaguchi, K.; Koga, N.; Iwamura, H. *J. Am. Chem. Soc.* **2002**, *124*, 450.
(15) Isobe, H.; Takano, Y.; Kitagawa, Y.; Kawakami, T.; Yamanaka, S.; Yamaguchi, K.; Houk, K. N. *J. Phys. Chem. A* **2003**, *107* (5), 682.
(16) Frisch, M. J.; Trucks, G. W.; Schlegel, H. B.; Scuseria, G. E.; Robb, M. A.; Cheeseman, J. R.; Zakrzewski, V. G.; Montgomery, J. A., Jr.; Stratmann, R. E.; Burant, J. C.; Dapprich, S.; Millam, J. M.; Daniels, A. D.; Kudin, K. N.; Strain, M. C.; Farkas, O.; Tomasi, J.; Barone, V.; Cossi, M.; Cammi, R.; Mennucci, B. C.; Pomelli, C.; Adamo, C.; Clifford, S.; Ochterski, J.; Petersson, G. A.; Ayala, P. Y.; Cui, Q.; Morokuma, K.; Rega, N.; Salvador, P.; Dannenberg, J. J.; Malick, D. K.; Rabuck, A. D.; Raghavachari, K.; Foresman, J. B.; Cioslowski, J.; Ortiz, J. V.; Baboul, A. G.; Stefanov, B. B.; Liu, G.; Liashenko, A.; Piskorz, P.; Komaromi, I.; Gomperts, R.; Martin, R. L.; Fox, D. J.; Keith, T.; Al-Laham, M. A.; Peng, C. Y.; Nanayakkara, A.; Challacombe, M.; Gill, P. M. W.; Johnson, B.; Chen, W.; Wong, M. W.; Andres, J. L.; Head-Gordon, C. M.; Replogle, E. S.; Pople, J. A. *Gaussian 98*, revision A.11.3; Gaussian, Inc.: Pittsburgh, PA, 2002.
(17) Becke, A. D. *J. Chem. Phys.* **1993**, *98*, 5648.
(18) Becke, A. D. *Phys. Rev. A* **1988**, *38*, 3098.
(19) Lee, C.; Yang, W.; Parr, R. G. *Phys. Rev. B* **1988**, *37*, 785.
(20) Stevens, W.; Basch, H.; Krauss, J. *J. Chem. Phys.* **1984**, *81*, 6026.
(21) Stevens, W. J.; Krauss, M.; Basch, H.; Jasien, P. G. *Can. J. Chem.* **1992**, *70*, 612.
(22) Cundari, T. R.; Stevens, W. J. *J. Chem. Phys.* **1995**, *98*, 5555.
(23) Allen, F. H.; Kennard, O. *Chem. Design Automation News* **1993**, *8*, 31.
(24) Huzinaga, S. *Gaussian Basis Sets for Molecular Calculations*; Elsevier. Amsterdam, Oxford, New York, Tokyo, 1984.
(25) Hay, P. J. *J. Chem. Phys.* **1977**, *66*, 4377.
(26) Hehre, W. J.; Ditchfield, R.; Pople, J. A. *J. Chem. Phys.* **1972**, *56*, 2257.
(27) Hariharan, P. C.; Pople, J. A. *Mol. Phys.* **1974**, *27*, 209.
(28) Ribas, J.; Escuer, A.; Monfort, M.; Vicente, R.; Cortes, R.; Lezama, L.; Rojo, T. *Cood. Chem. Rev.* **1999**, *193*, 1027.
(29) Vicente, R.; Escuer, A.; Ribas, J.; Fallash, M. S. E.; Solans, X.; Font-Bardia, M. *Inorg. Chem.* **1993**, *32*, 1920.
(30) Ribas, J.; Monfort, M.; Diaz, C.; Bastos, C.; Solans, X. *Inorg. Chem.* **1994**, *33*, 484.
(31) Chaudhuri, P.; Weyhermüller, T.; Bill, E.; Wieghardt, K. *Inorg. Chim. Acta* **1996**, *252*, 195.
(32) Escuer, A.; Vicente, R.; Fallah, M. S. E.; Solans, X.; Font-Bardia, M. *Inorg. Chim. Acta* **1996**, *247*, 85.
(33) Li, L.; Liao, D.; Jiang, Z.; Yan, S. *Polyhedron* **2000**, *19*, 1575.
(34) Deoghoria, S.; Sain, S.; Soler, M.; Wong, W. T.; Christou, G.; Bera, S. K.; Chandra, S. K. *Polyhedron* **2003**, *22*, 257.
(35) Lin, X.; Shen, Z.; Song, Y.; Xu, H.; Li, Y.; You, X. *Inorg. Chim. Acta* **2005**, *358*, 1963.
(36) Sain, S.; Bid, S.; Usman, A.; Fun, H.; Aromi, G.; Solans, S.; Chandra, S. K. *Inorg. Chim. Acta* **2005**, *12*, 358.
(37) Ruiz, E.; Cano, J.; Alvarez, S.; Alemany, P. *J. Am. Chem. Soc.* **1998**, *120*, 11122.
(38) Kitajima, N.; Hikichi, S.; Tanaka, M.; Moro-oka, Y. *J. Am. Chem. Soc.* **1993**, *115*, 5496.
(39) Chaudhuri, P.; Kuppers, H. J.; Wieghardt, K.; Gehring, S.; Haase, W.; Nuber, B.; Weiss, J. *J. Chem. Soc., Dalton. Trans.* **1988**, 1367.
(40) Ruiz, E.; Fortea, A. R.; Tercero, J.; Cauchy, T.; Massobrio, C. *J. Chem. Phys.* **2005**, *123*, 074102.
(41) Aebersold, M. A.; Kahn, O.; Bergerat, P.; Plantevin, O.; Pardi, L.; Gillon, B.; Seggern, I. v.; Tuczek, F.; Ohrstrom, L.; Grand, A.; Levievre-Berna, E. *J. Am. Chem. Soc.* **1998**, *120*, 5238.
(42) Kahn, O. *Molecular Magnetism*; VCH Publishers: Weinheim, 1993.